Stopped-Flow Analysis of CO and NO Binding to Inducible Nitric Oxide Synthase†

Husam M. Abu-Soud,* Chaoqun Wu, Dipak K. Ghosh, and Dennis J. Stuehr*

Department of Immunology, Lerner Research Institute, The Cleveland Clinic, Cleveland, Ohio 44195

Received September 26, 1997

ABSTRACT: The oxygenase domain (amino acids 1−498) of inducible nitric oxide synthase ($iNOS_{ox}$) is a hemeprotein that binds L-arginine (L-Arg) and tetrahydrobiopterin (H_4B). During NO synthesis, the heme iron must bind and activate O_2, but it also binds self-generated NO to form an inactive complex. To better understand how L-Arg and H_4B affect heme iron function in $iNOS_{ox}$, we utilized stopped-flow spectroscopy to study heme reactivity with CO and NO and the properties of the resulting CO and NO complexes. CO and NO binding to ferrous and ferric (NO only) $iNOS_{ox}$ and subsequent complex stability was studied under four conditions: in the absence of L-Arg and H_4B and in the presence of either or both molecules. Ferric $iNOS_{ox}$ without L-Arg or H_4B was dimeric and contained low-spin heme iron, while in H_4B- or L-Arg-saturated $iNOS_{ox}$, the heme iron was partially or almost completely high-spin, respectively. In the presence of L-Arg or H_4B, the rate of CO binding to ferrous $iNOS_{ox}$ was slowed considerably, indicating that these molecules restrict CO access to the heme iron. In contrast, rates of NO binding were minimally affected. Under all conditions, the off rates for CO and NO were very high as compared to other hemeproteins. The six-coordinate Fe^{II}−CO and -NO complexes that initially formed were unstable and converted either slowly (CO) or quickly (NO) to their respective 5-coordinate complexes. However, this transition was largely prevented by either L-Arg or H_4B and was reversed upon air oxidation of the complex in the presence of these molecules. Thus, H_4B and L-Arg both promote a conformational change in the distal heme pocket of $iNOS_{ox}$ that can greatly reduce ligand access to the heme iron. The ability of H_4B and L-Arg to prevent formation of a five-coordinate heme Fe−NO complex, along with the high off rates observed for NO, help explain why iNOS can remain active despite forming a complex with NO during its normal catalysis.

Nitric oxide (NO)[1] is produced in animals by the NO synthases (NOSs). Three isoforms of NOS have been characterized, and although they differ in their primary sequence and mode of expression (*1*−*4*), they are similar regarding catalysis and composition. For example, they catalyze a two-step oxidation of L-arginine (L-Arg) that initially generates N^{ω}-hydroxyarginine as an enzyme-bound intermediate (*5*−*7*) and NO plus citrulline as final products (*4*, *8*). All three NOS are homodimeric in their active forms with each subunit being comprised of an N-terminal oxygenase domain that binds heme, tetrahydrobiopterin (H_4B), and L-Arg, and a C-terminal reductase domain that binds FMN, FAD, calmodulin (CaM), and NADPH (*9*−*13*). During NO synthesis, the reductase domain functions to obtain electrons from NADPH and passes them to the oxygenase domain, where NO synthesis takes place (*4*, *14*−*19*). Each domain when expressed individually retains its native functions and properties (*9*, *11*, *13*, *20*, *21*). For example, the NOS oxygenase domains when expressed in insect cells or in *Escherichia coli* are dimeric, display normal binding affinity toward L-Arg and H_4B, and can catalyze NO and citrulline synthesis in either an H_2O_2-driven reaction or when provided with NADPH and their respective reductase domain (*9*, *21*, *22*), whereas the reductase domains when expressed in yeast or *E. coli* are monomeric and can transfer NADPH-derived electrons to artificial acceptors at rates that match the full-length native proteins (*13*, *21*).

A variety of evidence suggests the NOS heme plays a central role in catalysis (*6*, *23*−*25*). Electron transfer to the heme iron initiates NO synthesis from L-Arg or superoxide/H_2O_2 production in the absence of substrate (*14*−*16*, *19*, *26*). In both cases, the reaction likely involves O_2 binding to ferrous heme iron to form a Fe^{II}−O_2 complex, with subsequent oxygen activation steps occurring at the heme as established for the cytochromes P-450 (*27*). Indeed, recent characterization of Fe^{II}−O_2 neuronal NOS directly supports a heme-based oxygen activation pathway in the NOS (*25*). As for the cytochrome P-450s, the NOS heme iron is ligated to the protein through a cysteine thiolate (*13*, *28*−*33*) and can bind a variety of alternative molecules as sixth ligands, including CO (*23*, *24*, *33*, *34*), NO (*18*, *35*, *39*), CN^- (*36*), and imidazole (*37*, *38*). NO binding to the NOS heme is particularly relevant because two NOS isoforms generate

† Supported by National Institutes of Health Grant CA53914 to D.J.S. and by a grant from the American Heart Association to H.A.S. D.J.S. is an Established Investigator of the American Heart Association. This work was presented in Abstract form at the ASBMB meeting in San Francisco, CA, in May 1996 and at the Second International Conference on the Biology and Biochemistry of Nitric Oxide, UCLA, CA, in July 1996.

* To whom manuscript correspondence should be addressed: Immunology, NN1 The Cleveland Clinic, 9500 Euclid Avenue, Cleveland, OH 44195. Phone (216) 445-6950. Fax (216) 444-9329. E-mail: stuehrd@cesmtp.ccf.org.

[1] Abbreviations: NO, nitric oxide; NOS, NO synthase; $iNOS_{ox}$, oxygenase domain of mouse inducible NOS; H_4B, (6*R*,*S*)-5,6,7,8-tetrahydro-L-biopterin.

S0006-2960(97)02398-2 CCC: $15.00
Published on Web 02/24/1998

heme Fe−NO complexes during normal catalysis (*18, 39*), and this markedly reduces their steady-state activity and alters their O_2 response (*40*).

Substrate and H_4B must both bind to NOS to support NO synthesis (*5, 41*−*43*). Although neither coordinate as ligands to the heme iron, their binding markedly influences its properties. For example, L-Arg binding to H_4B-saturated neuronal NOS has been reported to shift the heme iron spin equilibrium toward high-spin (*36, 38, 44*), increase heme iron reduction (*36*), and alter its electronic properties (*45*), antagonize binding of NO, CN^-, and imidazole (*35*−*39*), decrease the rate of CO rebinding (*36, 46*), alter heme iron-bound ligands such as CO and NO (*35, 47*), and protect portions of the porphyrin ring against covalent modification by electrophiles generated within the active site (*48*). These findings are all consistent with L-Arg occupying space above the distal side of the heme in order to interact with activated oxygen species that are presumably generated at the heme iron. Recent work with H_4B-free or -deficient dimeric NOS expressed in bacteria show that its heme iron is either completely or predominantly six-coordinate low-spin and can bind bulky ligands such as DTT that are normally excluded from the active site (*13, 49*−*51*). H_4B binding partially shifts the heme iron spin equilibrium toward high spin, displaces heme iron ligands such as DTT (*50, 51*), stabilizes the heme iron-thiolate bond (*47*), and protects the porphyrin ring against alkylation in a pattern distinct from L-Arg (*48*). Together, these results indicate that L-Arg or H_4B have similar but not identical effects on the heme iron environment and suggest that conformational changes associated with their binding close up the distal heme pocket (*47*). In the current report, we utilize NO and CO as model ligands to further investigate how L-Arg and H_4B control heme iron reactivity and coordination structure in the oxygenase domain of inducible NOS ($iNOS_{ox}$).

MATERIALS AND METHODS

Materials. CO and NO gases were purchased from Matheson Gas products, Inc., and used without further purification. All reagents and materials were obtained from Sigma or from sources reported previously (*52, 53*).

Protein Purification. $iNOS_{ox}$ domain (amino acids 1−498) containing a six-histidine tag at its C terminus was overexpressed in *E. coli* using the PCWori vector and isolated as previously reported (*50, 54*). The protein as isolated was free of L-Arg and H_4B and was ∼85% dimeric as judged by gel filtration chromatography. The $iNOS_{ox}$ concentration was estimated based on an extinction coefficient previously reported (*54*).

Optical Spectroscopy and Rapid Kinetic Measurements. Optical spectra were recorded on a Hitachi 3010 UV−visible spectrophotometer, at 10 °C. Anaerobic spectra were recorded using septum-sealed quartz cuvettes that could be attached through a quick-fit joint to a vacuum system. The $iNOS_{ox}$ samples were made anaerobic by repeated cycles of evacuation and equilibrated with catalyst-deoxygenated N_2. Separate buffer solutions containing cofactors were evacuated and gassed with N_2 in a separate vessel and were transferred to stopped-flow instrument or to anaerobic cuvettes using gastight syringes. Cuvettes were maintained under N_2, CO, or NO positive pressure during spectral measurements. The kinetic measurements were carried out using a Hi-Tech stopped-flow apparatus (model SF-51) equipped for anaerobic work. Measurements were carried out at 10 °C and initiated by rapid mixing of a solution of $iNOS_{ox}$ (2 μM) in the absence or presence of L-Arg (2 mM) and/or H_4B (10 μM) with a solution containing different concentrations of CO or NO. The reactions were monitored at single wavelengths to monitor combination of $iNOS_{ox}$ with CO or NO. Signal-to-noise ratios were improved by averaging 7−10 individual traces. The time courses were fit by use of nonlinear least-squares method provided by the instrument manufacturer, as described previously (*25*). In some experiments, the stopped-flow instrument was attached to a rapid-scanning diode array device (Hi-Tech MG-6000) designed to collect 96 complete spectra in a specific time frame. The diode array detector was calibrated relative to five reference absorbance wavelengths of holmium oxide filter (Hy-I) at 362, 420, 446, 460, and 536 nm. Rapid scanning experiments involved mixing anaerobic solutions of $iNOS_{ox}$ NO complex with anaerobic buffer solutions containing 400 μM sodium dithionite, or solutions of dithionite-reduced $iNOS_{ox}$ with anaerobic solutions saturated with NO, at 10 °C.

Sample and Solution Preparation. In some cases, $iNOS_{ox}$ samples were incubated overnight in 40 mM Bis-Tris propane buffer, pH 7.4, containing 1 mM DTT, 50 μM H_4B and/or 5 mM L-Arg. Anaerobic 0.1 M Bis-Tris propane buffer, pH 7.4, containing various concentrations of CO or NO were prepared by mixing different volumes of buffer saturated with CO or NO gas at 21 °C with an anaerobic buffer solution. Saturating concentrations of CO and NO at 21 °C are approximately 1 and 2 mM, respectively.

RESULTS

Formation and Stability of $iNOS_{ox}$ Fe^{II}−CO Complexes. Our previous work suggested that cysteine thiolate coordination to heme iron of neuronal NOS was destabilized if the preparation was partially H_4B-free (*29*). We therefore investigated if L-Arg and H_4B alone or in combination could stabilize heme iron ligand structure of the Fe^{II}−CO complex of $iNOS_{ox}$. The insets of Figure 1, panels A−D, show the absorbance spectra obtained for ferric $iNOS_{ox}$ samples after an overnight dialysis in buffer alone or in buffer containing either 5 mM L-Arg, 50 μM H_4B, or a combination of both molecules. The $iNOS_{ox}$ dialyzed in buffer alone exhibited a Soret absorbance peak at 417 nm, indicating its heme iron was in a fully low-spin state (*13*). Samples equilibrated with L-Arg or H_4B alone exhibited broad Soret maxima centered near 400 nm, consistent with a mixture of high- and low-spin ferric heme iron (*13, 26*). A sample equilibrated with L-Arg and H_4B together exhibited a narrow Soret band centered at 398 nm, indicating predominantly high-spin heme iron, as observed for native $iNOS_{ox}$ under this condition (*11*). This confirms that L-Arg and H_4B can bind independently to $iNOS_{ox}$ and alter its heme iron environment.

Adding dithionite to the $iNOS_{ox}$ samples that were equilibrated in the presence or absence of L-Arg and H_4B caused immediate heme reduction in all cases as judged by a decrease in Soret peak absorbance and its shift to 414 nm (Figure 1, insets) (*15, 16*). No further spectral change was observed after 90 min under anaerobic conditions, indicating that ferrous $iNOS_{ox}$ is stable under each of the four conditions

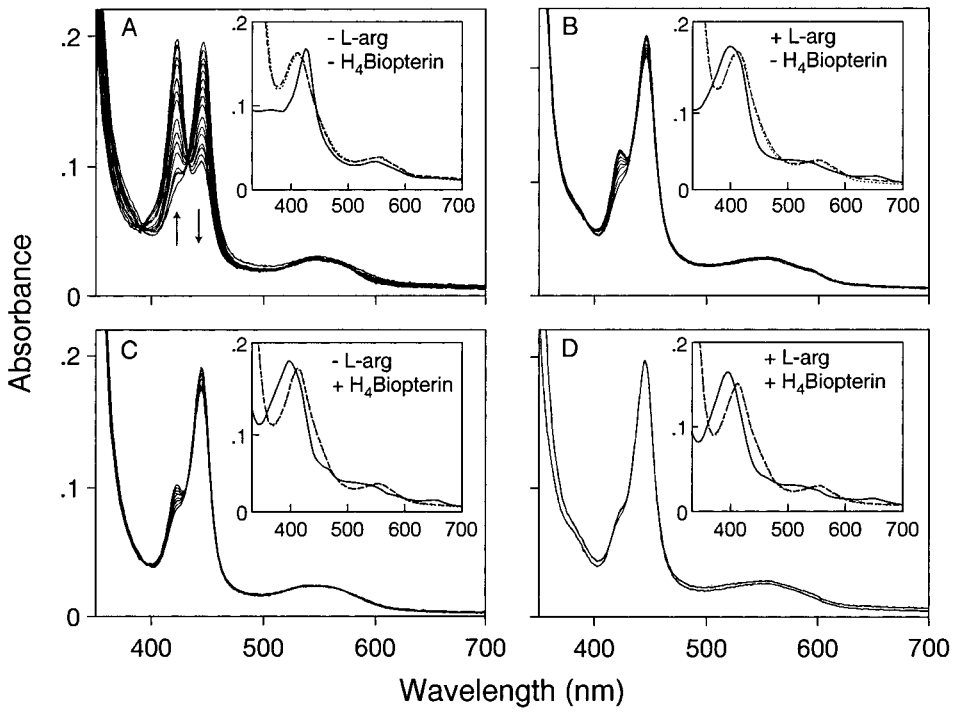

FIGURE 1: Light absorbance spectra of ferric $iNOS_{ox}$ and $Fe^{II}-CO$ $iNOS_{ox}$ complexes in the presence or absence of L-Arg and H_4B. Cuvettes contained 2 μM iNOSox under an anaerobic, CO saturated atmosphere at 10 °C in the presence or absence of 2 mM L-Arg and 10 μM H_4B, as noted in the inset of each panel. Enzyme was reduced by adding a slight excess of dithionite. Spectral traces were recorded immediately after reduction, and then after every 2−10 min for up to 5 h. Arrows in panel A indicate the direction of spectral change over time. Selected spectra were omitted from each panel for clarity. The insets show the spectra of ferric $iNOS_{ox}$ under the conditions noted in each panel (—), after adding dithionite to reduce $iNOS_{ox}$ heme iron (---), and 90 min after reduction (···). In some cases, the dashed and dotted lines were superimposed. The data are representative of four experiments.

(Figure 1, insets). Adding CO to the L-Arg- and H_4B-free ferrous $iNOS_{ox}$ (panel A) caused an immediate buildup of a CO complex with Soret absorbance maximum at 444 nm, but this species was unstable because its Soret peak gradually shifted to 421 nm over a 300 min time period at 10 °C. The spectral change suggests that cysteine thiolate coordination to the ferrous heme iron is destabilized upon binding CO under these conditions (*29*). Formation of the 421 nm $Fe^{II}-CO$ complex was not associated with conversion of dimeric $iNOS_{ox}$ into monomers, as determined by gel filtration (data not shown). $Fe^{II}-CO$ complexes of $iNOS_{ox}$ that were saturated with either L-Arg or H_4B showed much less conversion to the 421 nm species over the same time period (panels B and C), and an $iNOS_{ox}$ sample saturated with both L-Arg and H_4B showed no detectable conversion (panel D). The kinetics of spectral change associated with conversion of the 450 nm $Fe^{II}-CO$ complex to the 421 nm species under each of the four conditions is shown in Figure 2. On this basis, the conversion rate observed for the L-Arg- and H_4B-free $iNOS_{ox}$ $Fe^{II}-CO$ complex was best described by a single-exponential function with rate constant of 5.5×10^{-3} min^{-1} at 10 °C. Removing bound CO by degassing regenerated the original ferrous $iNOS_{ox}$ spectrum in all four cases. Some precipitation occurred upon degassing the $iNOS_{ox}$ sample that had completely converted to the 420 nm $Fe^{II}-CO$ species in the absence of L-Arg and H_4B. Furthermore, exposing the regenerated ferrous species to air generated the original ferric $iNOS_{ox}$ spectrum in all four cases, as shown for the −L-Arg/−H_4B and +L-Arg/+H_4B samples in Figure 3.

Kinetics of CO Binding. To examine how L-Arg and/or H_4B affect CO binding to ferrous $iNOS_{ox}$, we studied CO

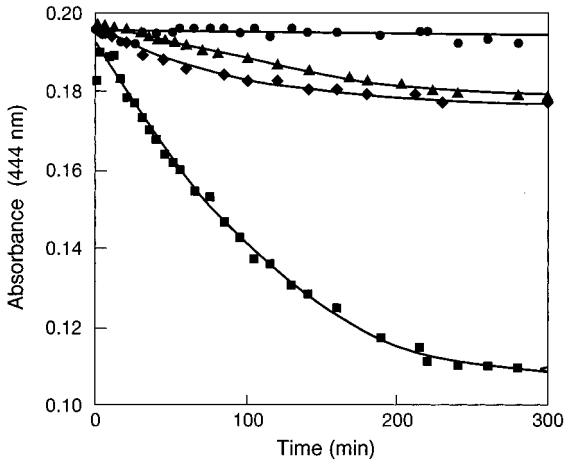

FIGURE 2: Effect of L-Arg and H_4B on the stability of the 444 nm $Fe^{II}-CO$ complex of $iNOS_{ox}$. The absorbance values at 444 nm from each spectral scan recorded in the experiments shown in the panels of Figure 1 are plotted versus time for $Fe^{II}-CO$ $iNOS_{ox}$ in the presence of H_4B and L-Arg (●), the presence of L-Arg (◆), the presence of H_4B (▲), and the absence of both L-Arg and H_4B (■).

binding using stopped-flow spectroscopy. Figure 4 contains representative stopped-flow traces of absorbance change at 444 nm versus time that were obtained in the presence of excess CO. In the absence of both L-Arg and H_4B (panel A), complex buildup was relatively fast and was best described by a single-exponential equation with an pseudo-first-order rate of 253 s^{-1}. When the same reaction was monitored over a longer time period, a slow decrease in absorbance at 444 nm was observed due to slow conversion to the 421 nm complex (data not shown). In the presence of H_4B, buildup of the $Fe^{II}-CO$ complex was biphasic and

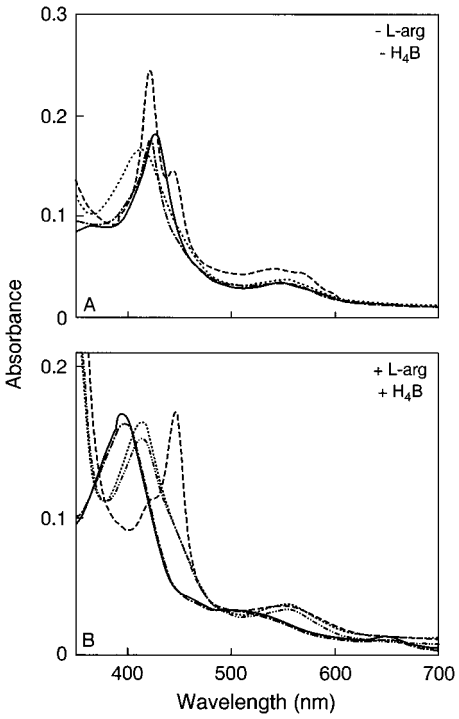

FIGURE 3: Reversiblity of $Fe^{II}-CO$ complex formation. Cuvettes contained 2 μM $iNOS_{ox}$ under an anaerobic atmosphere at 10 °C in the presence or absence of 2 mM L-Arg and 10 μM H_4B. Panel A shows $iNOS_{ox}$ as isolated in the absence of L-Arg and H_4B (—), after reduction by dithionite (•••), 2 h after adding CO to form the $Fe^{II}-CO$ complex (---), and after degassing the CO and exposing to air (-•-). Panel B shows $iNOS_{ox}$ in the presence of L-Arg and H_4B (—), after reduction by dithionite (•••), after adding CO to form the $Fe^{II}-CO$ complex (---), after degassing the CO under anaerobic conditions (••-), and exposing the $iNOS_{ox}$ solution to air (-•-).

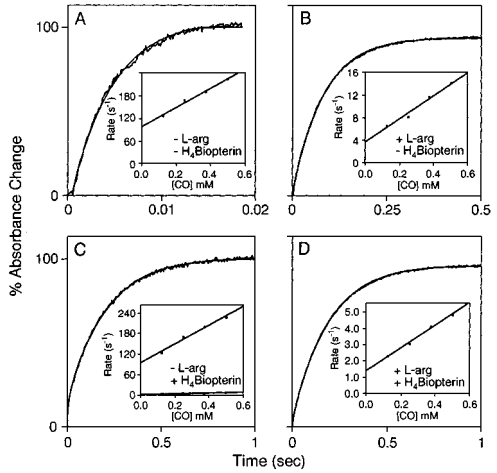

FIGURE 4: Stopped-flow analysis of CO binding to $iNOS_{ox}$ under various conditions. An anaerobic solution containing 2 μM ferrous $iNOS_{ox}$ and in some cases 4 mM L-Arg and/or 20 μM H_4B (as noted in the insets) was rapid mixed with a CO-saturated buffer solution at 10 °C, and the buildup of the $Fe^{II}-CO$ complex was monitored at 444 nm versus time. The smooth line in each trace represents the theoretical line of best fit. The insets contain plots of the observed rates of CO binding at different CO concentrations. The two lines present in inset C indicate that CO binding under this condition was biphasic. The data are representative of three or four separate experiments.

best fit to a two-exponential function with pseudo-first-order rates of 210 and 4.5 s^{-1}. Between 75 and 85% of the total absorbance change at 444 nm was associated with the slow phase. In the presence of L-Arg or L-Arg plus H_4B, buildup of the $Fe^{II}-CO$ complex was monophasic with pseudo-first-order rates of 16 and 5.4 s^{-1}, respectively. The reactions were repeated at different CO concentrations to obtain the second-order combination rate constants (k_{on}) and the first-order dissociation rates (k_{off}) for each of the four conditions. The insets of Figure 4 show the rate of spectral change as a function of CO concentration under each circumstance. In all cases, the plots were linear with positive intercept at the *y*-axis, indicating that CO binding is reversible and follows a simple one-step mechanism. The k_{on} and k_{off} values were derived from the graphs and are summarized in Table 1.

Table 1: Kinetics of CO and NO Binding to $iNOS_{Ox}$[a]

complex	condition	k_{on} (μM^{-1} s^{-1})	k_{off} (s^{-1})
$Fe^{II}-CO$	$-H_4B$ − L-Arg	0.25 ± 0.02	98 ± 5
	$-H_4B$ + L-Arg	0.021 ± 0.002	3.6 ± 0.6
	$+H_4B$ − L-Arg	0.23 ± 0.02	78 ± 6
		0.006 ± 0.001	2.1 ± 0.3
	$+H_4B$ + L-Arg	0.007 ± 0.0004	1.37 ± 0.11
$Fe^{II}-NO$	$-H_4B$ − L-Arg	1.82 ± 0.03	134 ± 4
	$-H_4B$ + L-Arg	1.40 ± 0.25	82 ± 28
	$+H_4B$ − L-Arg	0.69 ± 0.05	48 ± 9
	$+H_4B$ + L-Arg	0.67 ± 0.03	39 ± 3
$Fe^{III}-NO$	$-H_4B$ − L-Arg	0.059 ± 0.004	29 ± 3
	$-H_4B$ + L-Arg	1.57 ± 0.14	118 ± 22
	$+H_4B$ − L-Arg	1.34 ± 0.09	105 ± 10
	$+H_4B$ + L-Arg	0.99 ± 0.02	13 ± 3

[a] The combination of iNOSox and CO or NO was studied at 10 °C using single wavelength stopped-flow spectroscopy. The k_{on} and k_{off} values were derived by graphing k_{obs} versus ligand concentration.

Formation of Ferric− and Ferrous−Nitric Oxide Complexes. NO reacted with ferric $iNOS_{ox}$ in the absence or presence of L-Arg and H_4B to form a complex that displayed a Soret peak at 440 nm and two absorbance bands centered at 549 and 580 nm in all cases (Figure 5), consistent with a six-coordinate $Fe^{II}-NO$ complex (*28*). The $Fe^{II}-NO$ complexes were stable over time in the presence or absence of H_4B and L-Arg as judged by little or no detectable change in absorbance of the ferric $iNOS_{ox}$ NO complex over a 100 min range (Figure 5).

Addition of NO to the ferrous $iNOS_{ox}$ in the absence of L-Arg and H_4B initially formed a complex that displayed a Soret absorbance at 436 nm and a broad band centered at 576 nm (Figure 6), typical of the six-coordinate $Fe^{II}-NO$ complex (*28*), but this complex was extremely unstable and quickly converted to a species displaying a Soret band at 396 nm and a visible band at 580 nm (Figure 6). Under these conditions, the conversion in the absorbance Soret from 436 to 396 nm was biphasic and it was completed within 480 s.

The conversion to the 396 nm NO complex occurred both when NO was added to prereduced ferrous $iNOS_{ox}$ (as in Figure 6) and when the $Fe^{III}-NO$ complex was reduced with dithionite (Figure 7). In the latter case, the time course of this reaction was monitored over 1.6 s (Figure 7, panel A) or over 48 s (panel B), and the time course of absorbance change at 440 nm for each is shown in the insets of the panels. The absorbance change in the first part of the reaction collected over 1.6 s (upper panel inset) was best fit to a single-exponential function with a rate constant of 4.5 s^{-1}, while the change observed over the entire reaction was

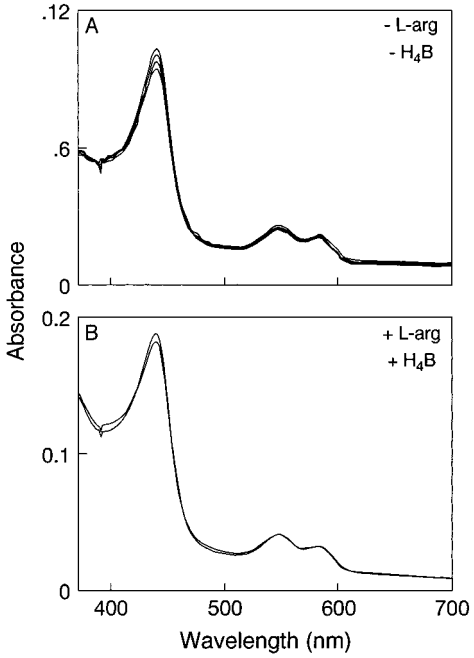

FIGURE 5: Light absorbance spectra of the ferric $iNOS_{ox}$ NO complex in the presence or absence of L-Arg and H_4B. Cuvettes contained 1−2 μM $iNOS_{ox}$ under an anaerobic NO saturated atmosphere at 10 °C in the absence (panel A) or presence of 2 mM L-Arg and 10 μM H_4B (panel B). Spectral traces were recorded immediately after NO addition, and then after every 2−10 min for up to 90 min. Some of the spectra recorded between the 0 and 90 min scans were omitted from each panel for clarity.

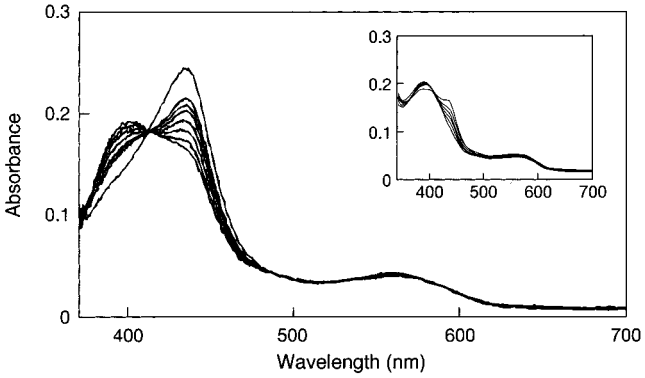

FIGURE 6: Formation of the $iNOS_{ox}$ Fe^{II}−NO complex and its conversion to the complex absorbing at 396 nm. Rapid-scanning diode array spectra were recorded during the reaction of dithionite-reduced $iNOS_{ox}$ (4 μM) with an anaerobic buffer solution containing NO (200 μM) at 10 °C. Ninety-six scans were collected over 480 s. Eight different spectra (0.0056, 40, 120, 200, 280, 320, 400, and 480 s) are shown for clarity. The first spectra corresponds with the initial formation of six-coordinate Fe^{II}−NO complex, which then converted to the 396 nm complex over time. The inset shows the same reaction as followed by conventional light absorbance spectroscopy. In this case, spectral traces were recorded immediately after NO addition and then after every 2 min for up to 30 min.

best fit to a two-exponential function with rate constants of 6.5 and 0.075 s^{-1} (lower panel inset). The overall reaction is complicated because it involves iNOSox heme reduction in addition to coversion of six-coordinate $iNOS_{ox}$ NO to the 396 nm complex. Conversion to the 396 nm NO complex was slowed in the presence of L-Arg or H_4B and did not occur at all in the presence of both molecules (data not shown), indicating L-Arg and H_4B stabilized the six-coordinate ferrous−NO complex of $iNOS_{ox}$.

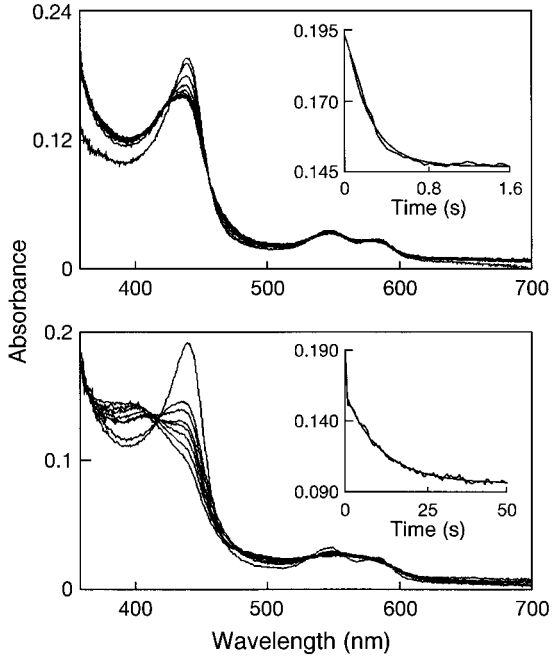

FIGURE 7: Reduction of Fe^{III}−NO $iNOS_{ox}$ and subsequent conversion to the 396 nm complex. The panels contain rapid-scanning diode array spectra recorded during the reaction of Fe^{III}−NO $iNOS_{ox}$ (4 μM) with a buffer solution that contains excess dithionite (600 μM). The time course of the reaction was monitored over 1.6 s (upper panel) or over 50 s (lower panel). Eight different selected spectra are shown in each panel for clarity. The insets show the kinetics of spectral change at 440 nm that occurs within the time frame of each panel. The time courses were fit to a single or double exponential function (solid line in upper and lower inset, respectively).

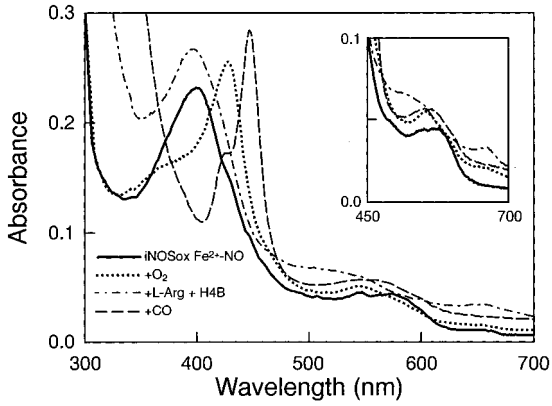

FIGURE 8: Capacity of the Fe^{II}−NO $iNOS_{ox}$ 396 nm complex to bind L-Arg and H_4B and regenerate an iron−thiolate bond following air oxidation. The cuvette contained an anaerobic buffer solution containing 2.5 μM $iNOS_{ox}$. A scan was recorded after the NO complex had fully converted to its 396 nm form ($iNOS_{ox}$ Fe^{2+}−NO). Excess NO gas was removed by purging with N_2, and a scan was recorded after the sample was oxidized by exposure to air (+O_2). L-Arg (2 mM) and H_4B (10 μM) were added and a scan recorded (+L-Arg + H_4B). The sample was then placed under an anaerobic CO atmosphere, reduced with dithionite, and a final scan recorded (+CO). The inset magnifies the five spectral scans in the region from 450 to 700 nm. The experiment shown is representative of two.

We next determined whether conversion to the 396 nm Fe^{II}−NO species irreversibly changed the heme iron ligand structure of $iNOS_{ox}$ or altered its ability to respond to L-Arg and H_4B. As shown in Figure 8, air oxidation of a preformed 396 nm Fe^{II}−NO complex generated a species whose

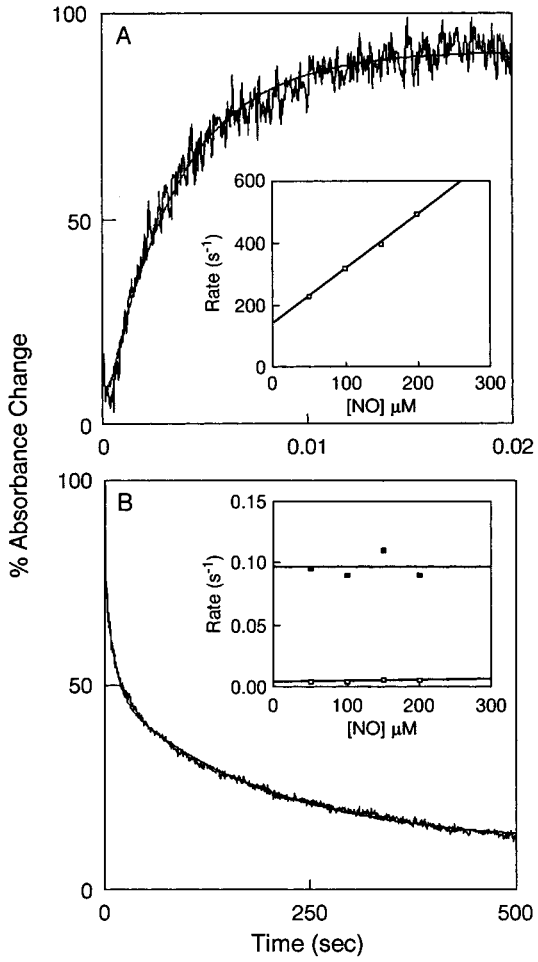

FIGURE 9: Kinetics of Fe^{II}−NO complex formation in the absence of L-Arg and H_4B and its conversion to the 396 nm complex. An anaerobic buffer solution containing 2 μM ferrous $iNOS_{ox}$ was rapid mixed with an anaerobic solution containing 200 μM NO at 10 °C. Panels A and B indicate absorbance change at 436 nm versus time. In panel A, buildup of the Fe^{II}−NO complex is monitored, while in panel B the subsequent conversion to the 396 nm complex is monitored. The smooth line in each trace is the theoretical line of best fit. The insets contain plots of the observed rates obtained at various NO concentrations. The two lines present in inset B indicate that conversion of the initial complex under this condition was biphasic. The data are representative of two identical experiments.

spectrum was identical to low-spin ferric $iNOS_{ox}$. Addition of L-Arg and H_4B to the sample caused a shift to a primarily high-spin form with Soret absorbance at 398 nm. Subsequent reduction with dithionite and exposure to CO generated a Fe^{II}−CO species that absorbed maximally at 444 nm, indicating that the ferrous heme iron was six-coordinate with a cysteine thiolate serving as the proximal axial ligand. Thus, we observed the original heme iron ligand structure and a normal response to L-Arg and H_4B after air oxidation of the 396 nm Fe^{II}−NO complex.

Kinetics of NO Binding and Conversion to the 396 nm Complex. Figure 9 contains stopped-flow traces of absorbance change at 436 nm versus time that were obtained at 10 °C when a solution containing excess NO was mixed with ferrous $iNOS_{ox}$ in the absence of both L-Arg and H_4B. Buildup of the initial complex absorbing at 436 nm is shown in panel A, while its subsequent conversion to the complex absorbing at 396 nm is shown in panel B. Buildup of the initial NO complex was monophasic and best fit to a single-exponential function with an observed rate constant of 295 s^{-1}, while subsequent conversion to the 396 nm complex was biphasic and best fit to a double exponential function, with observed rate constants of 0.096 and 0.0036 s^{-1}. A plot of the rate constants observed at different NO concentrations is shown as an inset in each panel of Figure 9. The plots are linear with positive intercept, indicating that formation of the initial Fe^{II}−NO complex and its subsequent conversion are reversible reactions that each proceed by a one-step mechanism. The rate at which the initial Fe^{II}−NO complex converted to the 396 nm complex was independent of the NO concentration. These experiments were repeated using $iNOS_{ox}$ samples equilibrated with L-Arg and/or H_4B. In all cases, the stopped-flow signals and results were qualitatively similar to the example shown in Figure 9A. The k_{on} and k_{off} values derived for NO binding to $iNOS_{ox}$ under the four various conditions are summarized in Table 1.

DISCUSSION

Expressing $iNOS_{ox}$ in *E. coli* enabled us to study how H_4B and L-Arg each affect heme iron ligand structure and reactivity with the diatomic ligands CO and NO. Although $iNOS_{ox}$ was free of L-Arg and H_4B, it was still 85% dimeric as judged by gel filtration chromatography and maintained a cysteine thiolate axial ligand, consistent with previous reports (*11*, *50*, *54*). The optical absorbance spectrum showed the heme iron was in a low-spin form, presumably indicating a water or hydroxide is present as a sixth ligand (*35*, *47*). Solvation of the distal pocket to generate low-spin heme iron is consistent with the pocket being able to accommodate a large ligand like DTT in the absence of L-Arg and H_4B (*50*, *51*) and suggests an open distal pocket exists in the $iNOS_{ox}$ dimer under such circumstances. H_4B or L-Arg altered the heme environment when provided alone or together, based on their partial or complete stabilization of high-spin ferric heme iron.

CO Binding to Ferrous $iNOS_{ox}$. Mixing ferrous $iNOS_{ox}$ with CO generated a six-coordinate Fe^{II}−CO complex in the presence or absence of L-Arg and H_4B, but the subsequent stability of this complex depended on the experimental conditions. Particularly in the absence of both L-Arg and H_4B, there was a slow but near quantitative conversion of the six-coordinate complex to one absorbing at 422 nm, which likely indicates breakage or weakening of the natural thiolate ligand provided by Cys194 (55) and possible substitution by an alternative ligand such as a histidine nitrogen (*29*). This conversion was to a large extent prevented either by bound L-Arg or H_4B, indicating an important role for these molecules in stabilizing the thiol−iron bond in the Fe^{II}−CO complex.

L-Arg and H_4B also appeared to restrict CO access to the ferrous heme iron as judged by their affects on CO binding rate. The rate observed in the absence of L-Arg and H_4B was decreased by a factor of 16 in the presence of L-Arg and by a factor of 40 in the presence of H_4B and L-Arg. In the presence of H_4B alone, two kinetically distinct species could be distinguished in that 15−25% of the heme iron bound CO at the original fast rate, and the rest bound CO slowly at a rate that was essentially equivalent to when both L-Arg and H_4B were bound. Our observing two kinetically distinct heme irons is consistent with flash photolysis (*36*,

46) and resonance Raman (*47*) studies done with other NOS isoforms that suggest at least two populations of $Fe^{II}-CO$ complex exist in samples saturated with H_4B alone. In the present case, when L-Arg was added to H_4B-saturated $iNOS_{ox}$ all of the heme iron appeared to convert to the slow binding species. The ability of L-Arg and H_4B to slow CO binding to $iNOS_{ox}$ is reminiscent of CO binding in cytochromes $P450_{cam}$ and $P450_{terp}$, where the substrates camphor and terpinol reduce the rate of CO binding 138- and 180-fold, respectively, (*56, 57*). However, this effect is not universal because substrate binding in cytochromes $P450_{LM4}$ and $P450_{LM2}$ has little or no effect on their CO combination rates (*58, 59*).

L-Arg and H_4B may decrease the rate of CO binding by constraining CO within the distal pocket of $iNOS_{ox}$. Studies of iron porphyrin model compounds such as Fe(TpivPP)(NMeIm)CO and Fe(TPP)(py)CO have shown that the $Fe^{II}-CO$ bond is linear in the absence of steric hindrance (*60, 61*). In heme proteins, the $Fe^{II}-CO$ bond is often bent due to steric constraints within the distal pocket. Forcing CO to adopt a bent geometry is thought to lower its binding affinity (*61*−*66*). For $iNOS_{ox}$, resonance Raman investigations suggest that CO is bound in a linear mode in the L-Arg- and H_4B-free form,[2] whereas it appears to bind in a bent mode in the presence of L-Arg and H_4B (*47*). This would explain our observation of a rapid rate of CO binding in the absence of L-Arg and H_4B and is consistent with this form of the $iNOS_{ox}$ dimer containing an open distal pocket that allows CO to bind unhindered. L-Arg and H_4B may constrain CO binding either by filling the space directly above the heme or by causing a protein conformational change that constricts the distal heme pocket.

CO dissociation from L-Arg- and H_4B-free $iNOS_{ox}$ was fast when compared with other hemeproteins, but was slower than CO dissociation from heme model compounds. For most heme proteins, CO dissociation from their respective 6-coordinate complexes ranges from 0.013 to 0.0002 s^{-1} (*64, 67*−*72*). Slow CO dissociation from the heme iron is though to be due to a positive trans effect contributed by the proximal ligand, which in many cases is a histidine nitrogen. However, there appear to be exceptions in that the CO dissociation rate from six-coordinate, histidine-ligated guanylate cyclase is 3.5 s^{-1} at 10 °C (*73*). Cytochrome $P\text{-}450_{cam}$ also exhibits a relatively faster rate of CO dissociation (2.3 s^{-1}, at 4 °C) (*57*), implying that a proximal thiolate ligand may have a weaker trans effect than an imidazole nitrogen. For protein-free compounds such as five-coordinate carboxyheme in cetyltrimethylammonium bromide detergent (*46*), the CO dissociation rate is only 4-fold higher than what we observed for $iNOS_{ox}$ in the absence of L-Arg and H_4B. Thus, fast CO dissociation in the absence of L-Arg and H_4B may be due to the thiolate axial ligand and an unusually open distal pocket. Alternatively, it may be due to the presence of a small fraction of five-coordinate complex, from which CO dissociation is rapid.

As seen for CO association to $iNOS_{ox}$ that contained only H_4B, CO dissociation occurred at a fast and a slow rate, indicating two species are present. L-Arg decreased CO dissociation rates in the absence or presence of H_4B by a factor of 12−40. A similar decrease was observed for $Fe^{II}-CO$ $P450_{cam}$ upon binding camphor, which is known to bind over the top of the heme (*57*). A steric effect upon L-Arg binding is easy to imagine given that crystal structure data indicate L-Arg likely binds in the distal pocket above the heme to interact with heme-generated reactive oxygen (*94*). However, we also saw that H_4B has a similar effect on slowing CO dissociation from a portion of $iNOS_{ox}$. Whether H_4B binds above the heme or indirectly causes a protein conformational change that restricts CO is still unknown.

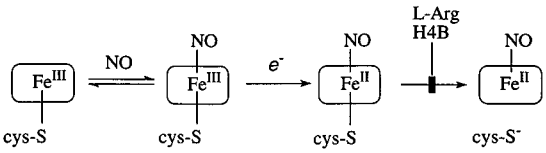

FIGURE 10: Model for NO binding to $iNOS_{ox}$. NO can bind to either ferric or ferrous $iNOS_{ox}$ and form a six-coordinate complex. The $Fe^{III}-NO$ complex is stable, while the $Fe^{II}-NO$ complex converts to a five-coordinate complex unless L-Arg and H_4B are present.

Together, the CO binding data indicate that L-Arg and H_4B play an important role in shaping the distal heme pocket in the $iNOS_{ox}$ dimer and suggest that in the absence of L-Arg or H_4B the distal pocket may minimally restrict ligand access to the heme. L-Arg and H_4B's capacity to constrain CO binding in the distal pocket is also associated with stabilization of the thiol−iron bond in the $Fe^{II}-CO$ complex.

NO Binding to Ferrous $iNOS_{ox}$. NO can bind to hemeproteins to form stable six-coordinate $Fe^{II}-NO$ complexes, or it can cause the trans axial ligand to weaken or break, thus forming five-coordinate $Fe^{II}-NO$ complexes (*74*−*80*). Three states are spectrally distinguishable by the position of the Soret band: six-coordinate NO complexes have a Soret band ranging from 427 to 440 nm (*18, 81, 82*), while those with a weakened or broken trans axial ligand bond exhibit Soret bands ranging from 417 to 420 nm (*75, 76*) and from 395 to 400 nm (*77*−*80*), respectively. In L-Arg and H_4B-free $iNOS_{ox}$, there was transient formation of a six-coordinate $Fe^{II}-NO$ complex (Soret absorbance at 436 nm) which quickly converted to another species whose Soret band position (396 nm) identifies it as the five-coordinate $Fe^{II}-NO$ complex of $iNOS_{ox}$. Indeed, its spectrum is identical with that of five-coordinate $Fe^{II}-NO$ model compounds (*77*−*80*). Thus, the $iNOS_{ox}$ dimer in the absence of L-Arg and H_4B behaves much like the cytochrome P-450s, which in general form unstable six-coordinate $Fe^{II}-NO$ complexes (*81, 83, 84*). Our stopped-flow studies have characterized the process for $iNOS_{ox}$ (Figure 10). The first step is reversible formation of the six-coordinate $Fe^{II}-NO$ complex whose rate is dependent on the NO concentration, while the second step is reversible breakage of the iron−thiolate bond whose rate is independent of the NO concentration. A similar model can describe CO binding and subsequent heme ligand rearrangement for ferrous $iNOS_{ox}$ in the absence of L-Arg and H_4B.

Spontaneous conversion of $Fe^{II}-NO$ $iNOS_{ox}$ from a six- to five-coordinate complex can be explained by the negative trans effect of NO (*81, 85, 86*) which favors cleavage of the iron-thiolate bond located on the opposite side of heme iron. The fact that this did not occur at all when L-Arg and H_4B were present together indicates these molecules completely

[2] J. Wang, personal communication.

stabilize the six-coordinate $Fe^{II}-NO$ complex of $iNOS_{ox}$. Because substrates cannot completely stabilize the six-coordinate forms of $Fe^{II}-NO$ cytochrome P450s (*81, 83, 84*), $iNOS_{ox}$ is a unique heme-thiolate protein in this respect.

The rate of NO binding to ferrous $iNOS_{ox}$ was decreased only 1.3−2.6-fold in the presence of L-Arg and H_4B, much less than the 12 to 42-fold rate decrease we observed for CO binding. The difference can be understood based on evidence obtained with sterically unhindered heme model compounds (*87*) and heme proteins such as hemoglobin A (*88*) or cytochrome *c* oxidase (*89*) which all show that a bent $Fe^{II}-NO$ bond is preferred. Apparently, in the presence of L-Arg and H_4B, the distal pocket of $iNOS_{ox}$ can better accommodate diatomic ligands that prefer to bind to the iron in a bent mode (NO), while those that prefer a linear mode (CO) are constrained. Similar considerations may explain why L-Arg and H_4B have only a small effect on the kinetics of O_2 binding to ferrous neuronal NOS (*25*), because O_2 also prefers to bind to the heme in a bent mode.

NO Binding to Ferric $iNOS_{ox}$. Kinetic studies with a number of heme proteins indicate that NO typically reacts faster with the ferrous rather than ferric form of the protein (*90*−*92*). However, this apparently is not the case for $iNOS_{ox}$, because the association rates of NO to its ferrous or ferric forms were similar, except in L-Arg- and H_4B-free $iNOS_{ox}$, where NO combination with the ferric form was much slower. The latter result is consistent with our light absorbance spectral data that show under this condition that the $iNOS_{ox}$ ferric heme iron is six-coordinate, low-spin in the absence of L-Arg and H_4B. Thus, NO binding would depend on initial displacement of the sixth ligand, which is likely to be water or hydroxide. An identical limitation on NO binding to other six-coordinate ferric heme proteins has been reported (*93*). In contrast, with H_4B or L-Arg, the $iNOS_{ox}$ heme iron is predominantly five-coordinate high-spin, and the unoccupied sixth position allows NO to bind directly to the $iNOS_{ox}$ ferric heme iron.

Our results indicate that the $Fe^{III}-NO$ complex of $iNOS_{ox}$ is more stable relative to the $Fe^{II}-NO$ complex, because in the absence of L-Arg and H_4B only 10−15% of the ferric complex converted to a five-coordinate form over a 1 h period as judged by the shift in the Soret absorbance from 440 to 395 nm. Thus, significant conversion to the five-coordinate NO complex is expected only under conditions where L-Arg and H_4B are deficient and the heme iron can be reduced either before or after binding NO. A similar result has been observed for neuronal NOS (*95*).

Implications. Our CO binding data suggest that L-Arg and H_4B have a profound effect on the $iNOS_{ox}$ distal heme pocket, converting it from a relatively open, unrestricted pocket to one that is constrained and only able to bind small heme iron ligands such as CO, NO, and O_2. The high rates of CO binding obtained in the absence of L-Arg and H_4B suggest that CO access to the $iNOS_{ox}$ heme is almost completely unrestricted under this condition. In addition, the magnitude of rate decreases caused by L-Arg or H_4B indicate that their relative capacities to restrict heme pocket access are somewhat similar, although their binding sites differ.

Our NO binding data impact on a fundamental aspect of catalysis that is unique to NOS, namely, their binding NO during normal aerobic catalysis. In neuronal NOS, a $Fe^{II}-NO$ complex forms during catalysis (*18*), while in iNOS, a $Fe^{III}-NO$ complex predominates (*39*).[3] Because NOS−NO complexes are catalytically inactive, their formation causes the enzymes to operate at only a fraction of their true maximum activity. We have proposed that NO complex formation controls the rate of NO synthesis during the steady state by setting up a condition in which the O_2-dependent breakdown of the NO complex becomes the rate-limiting step (*40*). Our current data will also enable a comparison of NO and O_2 binding to ferrous $iNOS_{ox}$, which may help explain how the enzyme partitions between its active and inactive forms during NO synthesis. In addition, we speculate that the high off-rates observed for NO complexes of iNOSox may be a key feature that drives decomposition of the enzyme−NO complex and promotes regeneration of ligand-free iNOS, which can again reduce its heme iron, bind O_2, and engage in productive catalysis.

ACKNOWLEDGMENT

We thank Pam Clark for excellent technical assistance.

REFERENCES

1. Brenman, J. E., Chao, D. S., Gee, S. H., McGee, A. W., Graven, S. E., Santillano, D. R., Wu, Z., Huang, F., Xia, H., Peters, M. F., Froehner, S. C., and Bredt, D. S. (1996) *Cell 84*, 757−767.
2. Nathan, C. F., and Xie, Q.-W. (1994) *J. Biol. Chem. 269*, 13725−13728.
3. Bredt, D. S., and Snyder, S. H. (1994) *Annu. Rev. Biochem. 63*, 175−195.
4. Griffith, O. W., and Stuehr, D. J. (1995) *Annu. Rev. Physiol.* 57, 707−736.
5. Stuehr, D. J., Kwon, N. S., Nathan, C. F., Griffith, O. W., Feldman, P. L., and Wiseman, J. (1991) *J. Biol. Chem. 266*, 6259−6263.
6. Klatt, P., Schmidt, K., Uray, G., and Mayer, B. (1993) *J. Biol. Chem. 268*, 14781−14787.
7. Pufahl, R. A., Nanjappan, P. G., Woodard, R. W., and Marletta, M. A. (1992) *Biochemistry 31*, 6822−6828.
8. Marletta, M. A. (1993) *J. Biol. Chem. 268*, 12231−12234.
9. Chen, P.-F., Tsai, A.-L., Berka, V., and Wu, K. K. (1996) *J. Biol. Chem. 271*, 14631−14635.
10. Masters, B. S. S., McMillan, K. Sheta, E. A., Nishimura, J. S., Roman, L. J., and Martasek, P. (1996) *FASEB J. 10*, 552−558.
11. Ghosh, D. K., Abu-Soud, H. M., and Stuehr D. J. (1996) *Biochemistry 35*, 1444−1449.
12. Xie, Q.-w., Cho, H. J., Kashiwabara, Y., Baum, M., Weidner, J. R., Elliston, K., Mumford, R., and Nathan, C. (1994) *J. Biol. Chem. 269*, 28500−28505.
13. McMillan, K., and Masters, B. S. S. (1995) *Biochemistry 34*, 3686−3693.
14. Abu-Soud, H. M., and Stuehr, D. J. (1993) *Proc. Natl. Acad. Sci. U.S.A. 90*, 10769−10772.
15. Abu-Soud, H. M., Yoho, L. L., and Stuehr, D. J. (1994) *J. Biol. Chem. 269*, 32047−32050.
16. Abu-Soud, H. M., Feldman, P. L., Clark, P., and Stuehr, D. J. (1994) *J. Biol. Chem. 269*, 32318−32326.
17. Heinzel, B., John, M., Klatt, P., Bohme, E., and Mayer, B. (1992) *Biochem. J. 281*, 627−630.
18. Abu-Soud, H. M., Wang, J., Rousseau, D. L., Fukuto, J., Ignarro, L. J., and Stuehr, D. J. (1995) *J. Biol. Chem. 270*, 22997−23006.
19. Pou, S., Pou, W. S., Bredt, D. S., Snyder, S. H., and Rosen, G. M. (1992) *J. Biol. Chem. 267*, 24173−24176.

[3] Preliminary work suggests this difference may be due to different rates of heme iron reduction in iNOS versus neuronal NOS (H. M. Abu-Soud, and D. J. Stuehr, unpublished results).

20. Sheta, E. A., McMillan, K., and Masters, B. S. S. (1994) *J. Biol. Chem. 269*, 15147−15153.
21. Gachhui, R., Presta, A., Bentley, D. F., Abu-Soud, H. M., McArthur, R., Brudvig, G., Ghosh, D. K., and Stuehr, D. J. (1996) *J. Biol. Chem. 271*, 20594−20602.
22. Ghosh, D. K., Abu-Soud, H. M., and Stuehr D. J. (1995) *Biochemistry 34*, 11316−11320.
23. McMillan, K., Bredt, D. S., Hirsch, D. J., Snyder, S. H., Clark, J. E., and Masters, B. S. S. (1992) *Proc. Natl Acad. Sci. U.S.A. 89*, 11141−11145.
24. Stuehr, D. J., and Ikeda-Saito, M. (1992) *J. Biol. Chem. 267*, 20547−20550.
25. Abu-Soud, H. M., Gachhui, R., Raushel, F. M., and Stuehr, D. J. (1997) *J. Biol. Chem. 272*, 17349−17353.
26. Gorren, A. C. F., List, B. M., Schrammel, A., Pitters, E., Hemmenes, B., Werner, E. R., Schmidt, K., and Mayer, B. (1996) *Biochemistry 35*, 16735−16745.
27. Groves, J. T., and Han, Y.-z. (1995) In *Cytochrome P450. Structure, Mechanism, and Biochemistry* (Ortiz de Montellano, P. R., Ed.) Plenum Press, New York, pp 3−48.
28. Wang, J., Rousseau, D. L., Abu-Soud, H. M., and Stuehr, D. J. (1995) *Proc. Natl. Acad. Sci. U.S.A. 91*, 10512−10516.
29. Wang, J., Stuehr, D. J., and Rousseau, D. L. (1995) *Biochemistry 34*, 7080−7087.
30. Wang, J., Stuehr, D. J., Ikeda-Saito, M., and Rousseau, D. L. (1993) *J. Biol. Chem. 268*, 22255−22258.
31. Chen, P.-F., Tsai, A.-L., and Wu, K. K. (1994) *J. Biol. Chem. 269*, 25062−25066.
32. Richards, M. K., and Marletta, M. A. (1994) *Biochemistry 33*, 14723−14732.
33. Sono, M., Stuehr, D. J., Ikeda-Saito, M., and Dawson, J. H. (1995) *J. Biol. Chem. 270*, 19943−19948.
34. White, K. A., and Marletta, M. A., (1992) *Biochemistry 31*, 6627−6631.
35. Wang, J., Rousseau, D. J., Abu-Soud, H. M., and Stuehr, D. J. (1994) *Proc. Natl. Acad. Sci U.S.A. 91*, 10512−10516.
36. Matsuoka, A., Stuehr, D. J., Olson, J. S., Clark, P., and Ikeda-Saito, M. (1994) *J. Biol. Chem. 269*, 20335−20339.
37. Wolf, D. J., Datto, G. A., Samatovicz, R. A., and Tempsick, R. A. (1993) *J. Biol. Chem. 268*, 9425−9429.
38. McMillan, K., and Masters, B. S. S. (1993) *Biochemistry 32*, 9875−9880.
39. Hurshman, A. R., and Marletta, M. A. (1995) *Biochemistry 34*, 5627−5634.
40. Abu-Soud, H. M., Rousseau, D. L., and Stuehr, D. J. (1996) *J. Biol. Chem. 271*, 32515−32518.
41. Kwon, N. S., Nathan, C. F., and Stuehr, D. J. (1989) *J. Biol. Chem. 264*, 20496−20501.
42. Tayeh, M. A., and Marletta, M. A. (1989) *J. Biol. Chem. 264*, 19654−19658.
43. Gross, S. S., and Levi, R. (1992) *J. Biol. Chem. 267*, 25722−25729.
44. Rodriguez-Crespo, I., Gerber, N. C., and Ortiz de Montellano, P. R. (1996) *J. Biol. Chem.* 11462−11467.
45. Salerno, J. C., Frey, C., McMillan, K., Williams, R. F., Masters, B. S. S., and Griffith, O. W. (1995) *J. Biol. Chem. 270*, 27423−27428.
46. Scheele, J. S., Kharitonov, V. G., Martasek, P., Roman, L. J., Sharma, V. S., Masters, B. S. S., and Magde, D. (1997) *J. Biol. Chem. 272*, 12523−12528.
47. Wang, J., Stuehr, D. J., and Rousseau, D. L. (1997) *Biochemistry 36*, 4595−4606.
48. Gerber, N. C., and Ortiz de Montellano, P. R. (1995) *J. Biol. Chem. 270*, 17791−17796.
49. Wu, C., Zhang, J., Abu-Soud, H. M., Ghosh, D. K., and Stuehr, D. J. (1996) *Biochem. Biophys. Res. Commun. 222*, 439−444.
50. Ghosh, D. K., Wu, C., Pitters, E., Molony, M., Werner, E. R., Mayer, B., and Stuehr, D. J. (1997) *Biochemistry 36*, 10609−10619.
51. Gorren, A. C. F., Schrammel, A., Schmidt, K., and Mayer, B. (1997) *Biochemistry 36*, 4360−4366.
52. Presta, A., Siddhanta, U., Wu, C., Sennequier, N., Huang, L., Abu-Soud, H. M., Eezurum, S., and Stuehr, D. J. (1998) *Biochemistry 37*, 298−310.
53. Sennequier, N., and Stuehr, D. J. (1996) *Biochemistry 35*, 5883−5892.
54. Siddhanta, U., Wu, C., Abu-Soud, H. M., Zhang, J., Ghosh, D. K., and Stuehr, D, J. (1996) *J. Biol. Chem. 271*, 7309−7312.
55. Xie, Q.-w., Leung, M., Fuortes, M., Sassa, S., and Nathan, C. (1996) *Proc. Natl. Acad. Sci. U.S.A. 93*, 4891−4896.
56. Sevrioukova, I. F., and Peterson, J. A. (1995) *Arch. Biochem. Biophys. 317*, 397−404.
57. Sligar, S. G., Filipovic, D., and Stayton, P. S. (1991) *Methods Enzymol. 206*, 31−49.
58. Narhi, L. O., and Fulco, A. J. (1986) *J. Biol. Chem. 261*, 7160−7169.
59. Boddupalli, S. S., Oster, T., Estabrook, R. W., and Peterson, J. A. (1992) *J. Biol. Chem. 267*, 10375−10380.
60. Hoard, J. L. (1975) in *Porphyrins and Metalloporphyrins* (Smith, K. M., Ed.) pp 356−358, Elsevier, New York.
61. Peng, S., and Ibers, J. (1976) *J. Am. Chem. Soc. 98*, 8032−8036.
62. Stryer, L. (1988) in *Biochemistry*, Freeman Publishing Co., San Francisco.
63. Caughey, W. S. (19970) *Ann. N. Y. Acad. Sci. 174*, 148−153.
64. Antonini, E., and Brunori, M. (1971) in *Hemoglobin and Myoglobin in Their Reactions with Ligands*, North-Holland Publishing Co., Amsterdam.
65. Heidner, E. J., Ladner, R. C., and Perutz, M. F. (1976) *J. Mol. Biol. 104*, 707−722.
66. Collman, J. P., Brauman, J., Halbert, T., and Suslick, K. (1976) *Proc. Natl. Acad. Sci. U.S.A. 73*, 3333−3337.
67. Gibson, Q. H., Olson, J. S., McKinnie, R. E., and Rohlfs, R. J. (1986) *J. Biol. Chem. 261*, 10228−10239.
68. Gibson, Q. H., Wittenberg, J. B., Wittenberg, B. A., Bogusz, D., and Appleby, C. A. (1989) *J. Biol. Chem. 264*, 100−107.
69. Rohlfs, R. J., Matthews, A. J., Carver, T. E., Olson, J. S., Springer, B. A., Egeberg, K. E., and Sligar, S. G. (1990) *J. Biol. Chem. 265*, 3168−3176.
70. Olson, J. S., Rohlfs, R. J., and Gibson, Q. H. (1987) *J. Biol. Chem. 262*, 12930−12938.
71. Gilles-Gonzalez, M. A., Gonzalez, G., and Perutz, M. F. (1994) *Biochemistry 33*, 8067−8073.
72. Kassner, R. J. (1991) *Biochim. Biophys. Acta 1058*, 8−12.
73. Stone, J. R., and Marletta, M. A. (1995) *Biochemistry 34*, 16397−16403.
74. Kon, H. (1975) *Biochim. Biophys. Acta 379*, 103−113.
75. Ascenzi, P., Brunori, M., Coletta, M., and Desideri, A. (1989) *Biochem. J. 258*, 473−478.
76. Yoshimura, T., and Ozaki, T. (1984) *Arch. Biochem. Biophys. 229*, 126−135.
77. Stone, J. R., and Marletta, M. A. (1994) *Biochemistry 33*, 5636−5640.
78. Gerzer, R., Bohme, E., Hofmann, F., and Schultz, G. (1981) *FEBS Lett. 132*, 71−74.
79. Tsai, A., Wei, C., and Kulmacz, R. J. (1994) *Arch. Biochem. Biophys. 313*, 367−372.
80. Yoshimura, T., Suzuki, S., Nakahara, A., Iwasaki, H., Masuko, M., and Matsubara, T. (1986) *Biochemistry 25*, 2436−2442.
81. O'Keeffe, D. H., Ebel, R. E., and Peterson, J. A. (1978) *J. Biol. Chem. 253*, 3509−3516.
82. Chiang, R., Makino, R., Spomer, W. E., and Hager, L. P. (1975) *Biochemistry 14*, 4166−4171.
83. Shiro, Y., Fujii, M., Iizuka, T., Adachi, S., Tsukamoto, K., Nakahara, K., and Shoun, H. (1995) *J. Biol. Chem. 270*, 1617−1623.
84. Tsubaki, M., Hiwatashi, A., Ichikawa, Y., Fujimoto, Y., Ikekawa, N., and Hori, H. (1988) *Biochemistry 27*, 4856−4862.
85. Trittelvitz, E., Gersonde, K., and Winterhalter, K. H. (1975) *Eur. J. Biochem. 51*, 33−42.
86. Henry, Y., Ishimura, Y., and Peisach, J. (1976) *J. Biol. Chem. 251*, 1578−1581.
87. Piciulon, P. L., Rupprecht, G., and Scheidt, R. W. (1974) *J. Am. Chem. Soc. 96*, 5293−5295.
88. Maxwell, J. C., and Caughey, W. S. (1976) *Biochemistry 15*, 388−396.

89. Barlow, C., and Erecinska, M. (1979) *FEBS Lett. 98*, 9−12.
90. Rose, E. J., and Hoffman, B. M. (1993) *J. Am. Chem. Soc. 105*, 2866−2873.
91. Sharma, V. S., Taylor, T. G., and Gardiner, R. (1987) *Biochemistry 26*, 3837−3843.
92. Radi, R. (1996) *Chem. Res. Toxicol. 9*, 828−835.
93. Traylor, T. G., and Sharma, V. S. (1992) *Biochemistry 31*, 2847−2849.
94. Crane, B. R., Arvai, A. S., Gachhui, R., Wu, C., Ghosh, D. K., Getzoff, E. D., Stuehr, D. J., and Tainer, J. A. (1997) *Science 278*, 425−431.
95. Migita, C. T., Saleno, J. C., Masters, B. S. S., Martasek, P., McMillan, K., and Ikeda-Saito, M. (1997) *Biochemistry 36*, 10987−10992.

BI972398Q